AIAA-95-1485-CP
A95- 26848

HYPERSONIC PANEL FLUTTER STUDIES ON CURVED PANELS

Ira Nydick*, Peretz P. Friedmann† and Xaolin Zhong ‡
Mechanical, Aerospace, and Nuclear Engineering Department
University of California, Los Angeles, CA 90095-1597

Abstract

The flutter of shallow, curved, heated three dimensional orthotropic panels exposed to hypersonic airflow is considered. The equations of motion, based on Marguerre shallow shell theory, are derived for two types of panel curvatures. The formulation also allows for the presence of a shock upstream of the panel and a general temperature distribution. The equations are solved using Galerkins method combined with direct numerical integration in time to compute stable limit cycle amplitudes. Nonsimple harmonic motions are observed for sufficiently high post-critical dynamic pressure values and the complex behavior is illustrated using representative phase plane plots. Aerodynamic heating, the presence of a shock in the flow, and nozero initial curvature are shown to significantly affect the aeroelastic behavior. A comparison of the aerodynamic loads predicted by 3rd order piston theory, the Euler equations and the Navier Stokes equations suggests that the solution of the fully coupled aerothermoelastic problem may be necessary to fully understand the aeroelastic behavior of a panel in hypersonic flow.

Nomenclature

a	Panel dimension in streamwise direction
a_∞	speed of sound
A_T	Coefficient of sinusoidal term of of imposed temperature distribution
b	Panel dimesion in spanwise direction
B_T	Coefficient of constant term of imposed temperature distribution
c_1, c_2, c_3	coefficients of hyperboloid representation of vehicle body
C_p	Pressure coefficient
C_T	Coefficient of streamwise linear term of imposed temperature distribution
D_x, D_y	Plate stiffness in the x and y directions, respectively
D_T	Coefficient of spanwise linear term of imposed temperature distribution
E_T	Coefficient of bilinear term of imposed temperature distribution
E_x, E_y	Moduli of elasticity in x,y directions respectively
F	Airy stress function
$\bar{F}$	Nondimensional Airy stress function, F/D_x
$\bar{F}_h, \bar{F}_p$	Homogeneous and particular parts of F
G_{xy}	Shear modulus

*Graduate Student Researcher, Student Member AIAA,ASME
†Professor, Fellow AIAA, Member AHS,ASME
‡Assistant Professor, Member AIAA

h	Panel thickness
L	Length of vehicle
M	Mach number
M_x^T, M_y^T	Thermal moment intensity resultants
N_x^T, N_y^T	Thermal stress intensity resultants
Q_A	Aerodynamic load
p	pressure
p_0	pressure in the panel cavity
$\bar{p}_1, \bar{p}_2, \bar{p}_3$	Nondimensional curvature coefficients in the quadratic/sine panel shape equation
s_1	Thru-thickness temperature coefficient
t	Time
$\bar{t}$	Nondimensional time used in ENO calculations
T	Temperature distribution on the panel
u^0	middle surface displacement in x direction
T_{nm}	Generalized coordinates of panel motion
v^0	middle surface displacement in y direction
V	Velocity of flow
$\bar{w}$	Nondimensional transverse panel displacement
x, y, z	coordinates for panel
$\bar{x}, \bar{y}, \bar{z}$	coordinates for vehicle surface
$\bar{Z}$	Shape of initially curved panel
$\bar{Z}_j$	Nondimensional curvature coefficients of the quadratic/sine panel shape
$\bar{Z}_{ij}$	Nondimensional curvature coefficients of the double sine panel shape
α_x, α_y	Coefficients of thermal expansion in x,y directions respectively
β	shock angle
ϵ	structural damping parameter
$\epsilon_{xx}^0, \epsilon_{yy}^0, \epsilon_{xy}^0$	middle surface strain components
γ	ratio of specific heats
θ_b	flow deflection angle
$\kappa_{xx}, \kappa_{yy}, \kappa_{xy}$	curvatures
λ	Nondimensional dynamic pressure, $\rho V_1^2 a^3 (D_x M_1)^{-1}$
λ_{cr}	Critical value of λ at which the linear system becomes unstable
μ	Air viscocity
$\tilde{\mu}$	$1 - \nu_{xy}\nu_{yx}$
ν_{xy}, ν_{yx}	Poisson ratios of orthotropic material
ξ, η	non-dimensional coordinates in the x and y directions
ρ	free stream air density
ρ_0	panel density
$\sigma_{xx}, \sigma_{yy}, \sigma_{xy}$	stress components
τ	Nondimensional time
$\dot{()}$	derivative with respect to time
$()_\infty$	value at undisturbed flow
$()_p$	value on the surface of piston
$()_1$	value behind the shock
$\tilde{()}$	nondimensional quantities
$()^*$	critical buckling value

1. Introduction

Renewed interest in the design of hypersonic vehicles motivated by the National Aerospace Plane (NASP), and its more recent successors, has generated a substantial number of new studies dealing with the aeroelastic, aerothermoelastic, and aeroservoelastic behavior of a vehicle representing a generic hypersonic configuration [1, 2, 3, 4]. While these studies are valuable, they have been based on a number of simplifying assumptions, the most restrictive of these being the use of linear piston theory [5] for calculating the aerodynamic loads.

Many papers have been published on panel flutter; however the emphasis in the majority of these studies was on the supersonic regime in

the range $2 < M < 4$. Furthermore, most of these papers have emphasized the case of flat panels using piston theory. Some more recent papers [6, 7, 8, 9, 10] have dealt in a somewhat cursory manner with panel flutter at hypersonic speeds involving aerodynamic heating using some simplifying assumptions. However, these papers have avoided some fairly important aspects of the problem, such as the panel location on the surface of the hypersonic vehicle and the validity of using piston theory in the hypersonic flight regime, which have been addressed in [11].

Flutter of curved isotropic panels has been studied by Dowell [12, 13] for both two dimensional (2D) and three dimensional (3D) configurations and more recently by Bismarck-Nasr [14]. A linear flutter analysis of 3D composite shells was performed by Pidiparti and Yang [15] using the finite element method.

This paper is a sequel to our previous paper [11] by introducing an improved formulation and solution process involving the type of curvatures that one would normally encounter on the surface of a hypersonic vehicle. It also differs from previous research in several important aspects: (1) The effect of shallow curvature is carefully incorporated into the derivation of the equations and it is shown that this significantly complicates the solution, which represents an aspect of the problem not noted previously; (2) thermal distributions are allowed both across the span as well as the thickness of the panel; (3) results obtained in a range of high dynamic pressure in the post-critical flutter region are shown to exhibit limit cycle behavior which has interesting characteristics not noted before; and (4) to assess the influence of the aerodynamic assumptions used, a comparison of piston theory with Euler solutions and a complete Navier-Stokes solution is also presented, generated for prescribed panel motion in hypersonic flow.

2. Formulation of the Problem

The geometry of the panel is shown schematically in Fig. 1, together with the external flow orientation. It is assumed that the panel is built of an orthotropic material characterized by four elastic constants E_x, E_y, ν_{xy} and ν_{yx}, and thermal expansion coefficients α_x, α_y, where the thermal expansion coefficient in the xy direction is assumed to be zero for the orthotropic case. The panel is loaded by a transverse aerodynamic load and is subject to a temperature change from the initial stress-free state.

In this study the structural model is based on an fairly straightforward extension of Marguerre plate theory [16] to include orthotropic panels. Marguerre plate theory can account for initial shallow curvature of the panel as well as geometric nonlinearity associated with moderate deflection, which is similar to Von Karman plate theory for flat plates. The plate equations contain terms associated with geometric nonlinearity, initial curvature, and the resultant coupling between them. The equations are derived for a general orthoropic panel. These equations are solved in nondimensional form, and thus the panel is characterized by the nondimensional quantities $E_y/E_x, G/E_x, \nu_{xy}, \nu_{yx}, \alpha_x$, and α_y.

The middle surface strains and curvatures of Marguerre plate theory are given by

$$\begin{aligned}
\epsilon^0_{xx} &= \frac{\partial u^0}{\partial x} + \frac{1}{2}\left(\frac{\partial w}{\partial x}\right)^2 + \frac{\partial Z}{\partial x}\frac{\partial w}{\partial x} \\
\epsilon^0_{yy} &= \frac{\partial v^0}{\partial y} + \frac{1}{2}\left(\frac{\partial w}{\partial y}\right)^2 + \frac{\partial Z}{\partial y}\frac{\partial w}{\partial y} \qquad (1) \\
\epsilon^0_{xy} &= \frac{\partial v^0}{\partial x} + \frac{\partial u^0}{\partial y} + \frac{\partial w}{\partial x}\frac{\partial w}{\partial y} + \frac{\partial Z}{\partial x}\frac{\partial w}{\partial y} + \frac{\partial Z}{\partial y}\frac{\partial w}{\partial x}
\end{aligned}$$

and

$$\begin{aligned}
\kappa_x &= -\frac{\partial^2 w}{\partial x^2} \\
\kappa_y &= -\frac{\partial^2 w}{\partial y^2} \qquad (2) \\
\kappa_{xy} &= -2\frac{\partial^2 w}{\partial x \partial y}
\end{aligned}$$

The stress-strain relations are given by

$$\begin{aligned}
\sigma_{xx} &= \frac{E_x}{\tilde{\mu}}\epsilon_{xx} + \frac{\nu_{xy}E_y}{\tilde{\mu}}\epsilon_{yy} - \frac{E_x}{\tilde{\mu}}\alpha_x T - \\
&\quad \frac{\nu_{xy}E_y}{\tilde{\mu}}\alpha_y T \\
\sigma_{yy} &= \frac{E_y}{\tilde{\mu}}\epsilon_{yy} + \frac{\nu_{xy}E_y}{\tilde{\mu}}\epsilon_{xx} - \frac{E_y}{\tilde{\mu}}\alpha_y T - \\
&\quad \frac{\nu_{xy}E_y}{\tilde{\mu}}\alpha_x T \qquad (3) \\
\sigma_{xy} &= G_{xy}\epsilon_{xy}
\end{aligned}$$

With these assumptions the equations of motion for the orthotropic panel can be written in the following manner.

$$\begin{aligned}
&D_x\frac{\partial^4 w}{\partial x^4} + 2(D_x\nu_{yx} + D_{xy})\frac{\partial^4 w}{\partial x^2\partial y^2} + D_y\frac{\partial^4 w}{\partial y^4} \\
&-\frac{\partial^2 F}{\partial y^2}\frac{\partial^2(w+Z)}{\partial x^2} - \frac{\partial^2 F}{\partial x^2}\frac{\partial^2(w+Z)}{\partial y^2} + \\
&2\frac{\partial^2 F}{\partial x\partial y}\frac{\partial^2(w+Z)}{\partial x\partial y} + \frac{\partial^2 M_x^T}{\partial x^2} + \\
&\frac{\partial^2 M_y^T}{\partial y^2} + \rho_0 h\frac{\partial^2 w}{\partial t^2} + \rho_0 h\epsilon\frac{\partial w}{\partial t} = \\
&Q_A(x,y,t) \qquad (4)
\end{aligned}$$

where F in Eq. (4) is the Airy stress function, given by

$$\begin{aligned}
&\frac{1}{E_y h}\frac{\partial^4 F}{\partial x^4} - \frac{2}{h}\left(\frac{\nu_{xy}}{E_x} - \frac{1}{2G_{xy}}\right)\frac{\partial^4 F}{\partial x^2\partial y^2} + \\
&\frac{1}{E_x h}\frac{\partial^4 F}{\partial y^4} + \frac{\partial^2 w}{\partial x^2}\frac{\partial^2 w}{\partial y^2} - \left(\frac{\partial^2 w}{\partial x\partial y}\right)^2 + \\
&\frac{\partial^2 Z}{\partial x^2}\frac{\partial^2 w}{\partial y^2} + \frac{\partial^2 Z}{\partial y^2}\frac{\partial^2 w}{\partial x^2} - 2\frac{\partial^2 Z}{\partial x\partial y}\frac{\partial^2 w}{\partial x\partial y} \\
&+\frac{1}{E_x h}\frac{\partial^2 N_x^T}{\partial y^2} + \frac{1}{E_y h}\frac{\partial^2 N_y^T}{\partial x^2} - \\
&\frac{\nu_{xy}}{E_x h}\left(\frac{\partial^2 N_y^T}{\partial y^2} + \frac{\partial^2 N_x^T}{\partial x^2}\right) = 0 \qquad (5)
\end{aligned}$$

where the following definitions have been used.

$$D_x = \frac{E_x h^3}{12\tilde{\mu}};\quad D_y = \frac{E_y h^3}{12\tilde{\mu}};\quad D_{xy} = \frac{G_{xy}h^3}{6}$$

The thermal stress and moment intensity resultants are given by

$$N_x^T = \int_{-\frac{h}{2}}^{\frac{h}{2}}\left(\frac{E_x}{\tilde{\mu}}\alpha_x + \nu_{xy}\frac{E_y}{\tilde{\mu}}\alpha_y\right)T\,dz \quad (6)$$

$$N_y^T = \int_{-\frac{h}{2}}^{\frac{h}{2}}\left(\frac{E_y}{\tilde{\mu}}\alpha_y + \nu_{xy}\frac{E_y}{\tilde{\mu}}\alpha_x\right)T\,dz \quad (7)$$

$$M_x^T = \int_{-\frac{h}{2}}^{\frac{h}{2}}\left(\frac{E_x}{\tilde{\mu}}\alpha_x + \nu_{xy}\frac{E_y}{\tilde{\mu}}\alpha_y\right)Tz\,dz \quad (8)$$

$$M_y^T = \int_{-\frac{h}{2}}^{\frac{h}{2}}\left(\frac{E_y}{\tilde{\mu}}\alpha_y + \nu_{xy}\frac{E_y}{\tilde{\mu}}\alpha_x\right)Tz\,dz \quad (9)$$

The boundary conditions associated with this problem are those corresponding to a simply supported plate along its four edges. It should also be noted that the Marguerre equations for a shallow curved panel are appropriate when the criterion for shallowness is defined as $(h/R_c) < 0.02$, where R_c is a representative radius of curvature.

2.1 Aerodynamic Load

Accurate representation of the unsteady aerodynamic load in hypersonic flow is quite difficult because high temperature effects, viscosity, and a chemically reacting boundary layer can be important. The aerodynamic loads in this study are obtained assuming inviscid,continuum hypersonic flow over a slender body. In this case the shock wave lies close to the body and the shock angle is small. Third order piston theory[5], given by Eq.(10), is used to calculate the aerodynamic load; and the validity of this assumption is examined later in the paper.

$$\begin{aligned}
Q_A(x,y,t) &= (p_0 - p_1) - p_1\left[\gamma\frac{v_p}{a_1} + \right. \\
&\left.\frac{\gamma(\gamma+1)}{4}\left(\frac{v_p}{a_1}\right)^2 + \frac{\gamma(\gamma+1)}{12}\left(\frac{v_p}{a_1}\right)^3\right] \quad (10)
\end{aligned}$$

where

$$v_p = a_1 M_1\left(\frac{\partial Z}{\partial x} + \frac{\partial w}{\partial x} + \frac{1}{V_1}\frac{\partial w}{\partial t}\right)$$

The values of the flow parameters behind the shock may be calculated using the oblique shock relations given by [17]

$$\begin{aligned}
\frac{p_1}{p_\infty} &= 1 + \frac{2\gamma}{\gamma+1}[(M_\infty\sin\beta)^2 - 1] \\
\frac{\rho_1}{\rho_\infty} &= \frac{(\gamma+1)(M_\infty\sin\beta)^2}{(\gamma-1)(M_\infty\sin\beta)^2 + 2}
\end{aligned}$$

$$\frac{a_1}{a_\infty} = \sqrt{\frac{p_1\rho_\infty}{p_\infty\rho_1}}$$

$$M_1 = \frac{1}{\sin(\beta-\theta_b)}\sqrt{\frac{(M_\infty\sin\beta)^2+\frac{2}{\gamma-1}}{\frac{2\gamma}{\gamma-1}(M_\infty\sin\beta)^2-1}} \quad (11)$$

where β is obtained from

$$\tan\theta_b = 2\cot\beta\left[\frac{(M_1\sin\beta)^2-1}{M_1^2(\gamma+\cos 2\beta)+2}\right] \quad (12)$$

Equation (12) may be solved for β for a given value of θ_b. There are two solutions for β; the "weak shock" solution is chosen because it is the physically correct one for the region of the vehicle located far from the blunt nose. In this region, the flow deflection angle is small and the shock angle approaches the mach angle, which is the limiting weak shock solution for small θ_b [17]. The oblique shock relations may be simplified in the case of hypersonic flow [18] using the hypersonic similarity parameter, $K = M_\infty\theta_b$, so that β is given as an explicit function of K. However, the exact relations are used in this study because only minor additional programming effort is required for their implementation.

Determining the range of validity of piston theory, when compared to more refined theories based on computational fluid dynamics (CFD), is an important question which is addressed in in a later section, where piston theory is compared to both the Euler equations and the Navier-Stokes equations. Also, while the use of the oblique shock relations is justified by the exploratory nature of this study, the presence of high temperature and real-gas effects in the flow over a hypersonic vehicle may significantly modify the the properties of the shock.

2.2 Temperature Distribution

The aerodynamic model used in this study is based on the assumption that there is no interaction between the flow and the panel temperature and the vehicle is flying at constant speed. Temperature effects due to aerodynamic heating are included by prescribing a temperature distribution given by

$$T = A_T\sin(\pi\bar{x})\sin(\pi\bar{y})(s_1\bar{z}+\frac{1}{2}) + B_T + C_T\bar{x} + D_T\bar{y} + E_T\bar{x}\bar{y} \quad (13)$$

This contains a through the thickness variation of the sinusoidal term which results in nonzero thermal moments experienced by the panel. The effect of any term in the temperature distribution represented by Eq. (13) on the flutter behaviour is determined by setting all but that particular coefficient to zero.

The critical buckling temperature for a flat, simply supported orthotropic plate exposed to a uniform temperature distribution is given by

$$T^*(m,n) = \frac{\pi^2}{12}\left(\frac{h}{a}\right)^2 \cdot \frac{\left[m^4+2(\nu_{yx}+2\tilde{\mu}\frac{G_{xy}}{E_x})\left(\frac{a}{b}\right)^2m^2n^2+\frac{E_y}{E_x}\left(\frac{a}{b}\right)^4n^4\right]}{\left[(\alpha_x+\nu_{yx}\alpha_y)m^2+\left(\frac{E_y}{E_x}\alpha_y+\nu_{yx}\alpha_x\right)\left(\frac{a}{b}\right)^2n^2\right]} \quad (14)$$

For a given orthotropic panel, T^* is determined by evaluating Eq. (14) for increasing combinations of the integers m, n starting from $m, n = 1$ and choosing the smallest value of $T^*(m,n)$. For a square isotropic panel, the lowest value occurs for $m, n = 1$ and is given by

$$T^* = \frac{\pi^2}{6}\left(\frac{h}{a}\right)^2\frac{1}{\alpha(1+\nu)}$$

The critical buckling temperature for a curved panel may be obtained numerically by generating time history data for the heated, curved panel with the aerodynamic load equal to zero, and increasing the temperature until static buckling is observed.

2.3 Mathematical Description of Initial Curvature

A panel located on the surface of a hypersonic vehicle will in general posess a small amount of initial curvature, as shown in Fig. 2. Two mathematical descriptions of the initial panel shape are used in this study, as represented by Eqs. (15) and (16), respectively

$$\bar{Z} = \frac{1}{2}(\bar{p}_1\xi^2+\bar{p}_2\xi+\bar{p}_3)\sum_{j=1}^{J}\bar{Z}_j\sin(j\pi\bar{\eta}) \quad (15)$$

$$\bar{Z} = \sum_{i=1}^{I}\sum_{j=1}^{J}\bar{Z}_{ij}\sin(i\pi\bar{\xi})\sin(j\pi\bar{\eta}) \quad (16)$$

where $\bar{Z} = Z/h$, $\xi = x/a$, and $\eta = y/b$. Equation (15) implies a parabolic panel shape variation in the y-direction and a sinusoidal variation in the x-direction that closely approximates the curvature of a panel located on the surface of a generic hypersonic vehicle. The coefficients, $\bar{p}_1$-$\bar{p}_3$, are obtained by fitting an analytical expression which approximates the shape of a generic hypersonic vehicle to the dimensions of the NASP Demonstrator model [3] and performing a change of coordinates to a local system located at the desired position on the vehicle body. An analytical expression which approximates such a configuration is a hyperboloid of two sheets, described by

$$\left(\frac{\bar{x}+c_1}{c_1}\right)^2 - \frac{\bar{y}^2}{c_2^2} - \frac{\bar{z}^2}{c_3^2} = 1 \quad (\bar{x} > 0) \qquad (17)$$

which represents a hyperboloid shifted on the $\bar{x}$-axis such that the vertex of the right surface is located at the origin. The parameters c_1, c_2, and c_3, which determine the dimensions of the hyperboloid, are selected so as to resemble the dimensions of the NASP (considered as a generic hypersonic vehicle). The algebraic steps required to obtain the expression for the vehicle body as a function of the local coordinates of the panel are quite lengthy and the details are omitted here.

The double sine series description of the initial panel geometry, Eq.(16), is included for comparison purposes and as another possible shape for a curved panel.

3. Method of Solution

The resulting nonlinear partial differential equations are solved using the global Galerkin method which has been frequently used for this class of problems [19, 20, 21, 22]. It is assumed that the panel is simply supported; this assumption simplifies the choice of the shape functions and it also produces conservative stability boundaries.

$$\bar{w}(\xi,\eta,\tau) = \sum_{i=1}^{I}\sum_{j=1}^{J} \bar{T}_{ij}(\tau)\sin(i\pi\xi)\sin(j\pi\eta) \qquad (18)$$

where

$$\bar{w} = \frac{w}{h},\ \bar{T}_{ij} = \frac{T_{ij}}{h},\ \tau = \frac{t}{\sqrt{\rho_0 h a^4 D_x^{-1}}}$$

The solution procedure consists of two parts, finding a solution for the nondimensionalized Airy stress function $\bar{F}(\xi,\eta) = F/D_x$, and then applying Galerkin's method to obtain a set of nonlinear ordinary differential equations. The Airy stress function which satisfies Eq.(5) consists of a homogeneous part, $\bar{F}_h$ and a particular part, $\bar{F}_p$. The particular solution is obtained first, and must reproduce all the terms on the right hand side of Eq.(5) when substituted into the left hand side. The mathematical details of obtaining the particular solution as well as the implementation of Galerkin's method for producing a system of ordinary differential equations in time are quite lengthy. For the convenient curvature representation given by Eq.(16), manual derivation of the appropriate terms is feasible. However, for the curvature given by Eq.(15) the algebraic manipulations required the use of the symbolic software Macsyma [23].

The homogenous solution satisfies Eq.(5) with the right hand side set to zero. This is obtained by assuming a solution in the form

$$\bar{F}_h(\xi,\eta) = \frac{1}{2}(C_1\xi^2 + C_2\eta^2 + C_3\xi\eta) \qquad (19)$$

The coefficients C_1, C_2, and C_3 are obtained by enforcing the in-plane boundary conditions, which imply zero mean shear and zero mean displacements at the panel boundaries [19]. For the curvature representation given by Eq.(16), one obtains

$$\begin{aligned} C_1 &= \frac{3\pi^2}{2}\frac{E_y}{E_x}\sum_{i=1}^{I}\sum_{j=1}^{J}\left[\left(\nu_{xy}i^2 + \left(\frac{a}{b}\right)^2 j^2\right)\right. \\ &\quad \left.\left(\bar{T}_{ij}{}^2 + 2\bar{Z}_{ij}\bar{T}_{ij}\right)\right] - 12\left(\frac{a}{h}\right)^2 \nu_{yx} I_1^T \\ &\quad -12\left(\frac{a}{h}\right)^2 \frac{E_y}{E_x} I_2^T \\ C_2 &= \frac{3\pi^2}{2}\sum_{i=1}^{I}\sum_{j=1}^{J}\left[\left(i^2 + \nu_{yx}\left(\frac{a}{b}\right)^2 j^2\right)\right. \end{aligned}$$

$$\left(\bar{T}_{ij}{}^2 + 2\bar{Z}_{ij}\bar{T}_{ij}\right)\Bigg] - 12\left(\frac{a}{h}\right)^2 I_1^T$$
$$-12\left(\frac{a}{h}\right)^2 \nu_{yx} I_2^T$$
$$C_3 = 0 \qquad (20)$$

where

$$I_1^T = \frac{A_T\gamma_T}{\pi^2\tilde{\mu}}\left[\nu_{xy} - \left(\frac{a}{b}\right)^2\right] + \delta_T[(\alpha_x + \nu_{yx}\alpha_y) - \nu_{yx}(\alpha_y + \nu_{xy}\alpha_x)]$$

$$I_2^T = \frac{A_T\gamma_T E_x}{\pi^2\tilde{\mu}E_y}\left[\left(\frac{a}{b}\right)^2\nu_{yx} - 1\right] + \delta_T[(\alpha_y + \nu_{xy}\alpha_x) - \nu_{xy}(\alpha_x + \nu_{yx}\alpha_y)]$$

$$\gamma_T = \left[(\alpha_x + \nu_{yx}\alpha_y)\left(\left(\frac{a}{b}\right)^2 - \nu_{xy}\right) + (\alpha_y + \nu_{xy}\alpha_x)\left(1 - \nu_{yx}\left(\frac{a}{b}\right)^2\right)\right]\left[\frac{E_x}{E_y} - 2\left(\frac{a}{b}\right)^2\left(\nu_{xy} - \frac{E_x}{2G_{xy}}\right) + \left(\frac{a}{b}\right)^4\right]^{-1}$$

$$\delta_T = \frac{1}{\tilde{\mu}}\left(\frac{A_T}{\pi^2} + B_T + \frac{C_T}{2} + \frac{D_T}{2} + \frac{E_T}{4}\right)$$

The expressions for the corresponding coefficients for initial curvature given by Eq.(15) are very lengthy and so are the mathematical details associated with finding the particular solution corresponding to both curvature expressions. An outline of this solution can be found in [19]; however the details are not presented here

Next the solution for $\bar{F}$ and the assumed solution for $\bar{w}(\xi,\eta,\tau)$, Eq.(18), are substituted into the equation of motion, Eq.(4), and the aerodynamic loading term, Eq.(10), after appropriate nondimensionalization. The spatial dependence is removed by applying Galerkin's method. When implementing Galerkin's method, N_l modes are used in the x-direction and N_w modes are used in the y-direction, which is perpendicular to the flow direction. The solution is sensitive to the number of modes used and therefore the convergence as a function of the number of modes is also considered. The resulting coupled ordinary nonlinear differential equations for the modal coefficients, T_{rs}, are solved by direct numerical integration on a digital computer. The numerical integration routine used in this study was DDEABM, a code based upon the Adams PECE formulas [24].

4. Alternative Representation of the Aerodynamic Load

Piston theory, which was developed for inviscid, isentropic, and perfect-gas supersonic flows, has been used to model the unsteady aerodynamic loads in many recent aeroelastic studies involving the hypersonic regime. However, practical hypersonic flow fields are viscous and sometimes require the treatment of real gas effects. The viscous effect is important for flow inside the boundary layer, and the real gas effects become important when the gas temperature is higher than about 1000^oK [18], which is often the case for hypersonic flow over practical aerospace vehicles. Therefore, the validity and range of application of piston theory for hypersonic flow applications needs to be carefully examined.

In this paper, we assess the validity of piston theory by comparing it with results obtained from solutions of the complete Euler and Navier-Stokes equations in a two-dimensional panel problem with a prescribed wall motion. Figure 3 shows a schematic of the two-dimensional hypersonic flow field used to validate the piston theory. The free-stream Mach number is 10.05, and the Reynolds number is 3.83×10^6. The panel oscillates with a prescribed motion given by $y = A\sin\frac{\pi n x}{L}\sin\omega t$, where $A = 0.002m$, $\omega = 1.206 \times 10^3 rad/sec$, $n = 2$, and $L = 0.45m$. The gas is assumed to be a perfect gas with $\gamma = 1.4$, and the viscosity coefficient of the gas is computed by the Sutherland formula.

The results of the compressible Navier-Stokes equations, which include both the momentum and energy equations in conservation law forms, are presented in this paper along with the results of the Euler solutions reported in a pre-

vious paper [11]. The Navier-Stokes equations are solved by the explicit second-order time-accurate essentially nonoscillatory (ENO) schemes [25]. More details of the numerical method and the validation of the computer code can be found in [26]. The boundary conditions used in the computations were described in [11]. For the Navier-Stokes equations, non-slip and isothermal boundary conditions are used on the panel surface. A 258×290 Cartesian grid and a CFL number of 0.5 are used in the computations.

Figure 4 shows the pressure coefficient on the mid-panel surface as a function of the nondimensional time defined by $\bar{t} = \omega t/80$. The solutions of the first-, second-, and third-order piston theory are compared with those from the Euler and Navier-Stokes equations. The results show that the nonlinear second- and third-order piston theory compares very well with the solutions from the unsteady Euler equations, and the linear first-order piston theory is not accurate enough for the present test problem. However, the Navier-Stokes solutions predict a much lower surface pressure than the Euler equations or piston theory. The viscosity in the boundary layer has a damping effect on the surface pressure because the surface motion occurs mainly within the boundary layer, which serves as a buffer zone between the external flow and the vibrating wall.

These results show that more accurate aerodynamic models are needed to account for the viscous effect in the boundary layer. One possible method is to model the boundary layer as a modified wall surface to account for the boundary layer thickness. The modified model can be checked by numerical computations of the full Navier-Stokes equations. Similarly, an aerodynamic model to account for the high temperature real gas effects can also be checked by the numerical simulation of the Navier-Stokes equations with real gas effects.

5. Results and Discussion

The majority of results obtained in this study are presented in the form of stable limit cycle amplitudes as a function of the non-dimensional dynamic pressure, λ. Typical limit cycle curves are obtained by calculating 5-8 amplitudes for values of the dynamic pressure parameter, λ, beyond the value of λ_{cr}, which represents the critical dynamic pressure at which the linear system becomes unstable. An example of this type of plot is shown in Fig. 5., which compares limit cycle curves for both isotropic and orthotropic panels with results given in previous studies. Results for the isotropic case were taken from Fig. 19 of [21] and those of the orthotropic case were taken from Fig. 3 of [10], converted to the nondimensional dynamic pressure definition employed in this study. Overall, the agreement in both cases is quite good.

To ensure that temperature effects are correctly incorporated in the formulation, results for an isotropic panel subject to uniform temperature rises of $T/T^* = 0.5$ and 1.0 were generated and compared with data from [21]. The plot shown in Fig. 6 shows excellent agreement. The data used for the validation studies shown in Figs. 5 and 6 is given in Table 1.

Properties used in this study for both isotropic and orthotropic panels are displayed in Table 2. Unless stated otherwise, the properties listed in the table were used for generating the results described. Atmospheric properties were taken at an altitude of 90,000 ft because it corresponds to $M = 10$, for a hypothetical flight trajectory of the NASP X-30 vehicle [1]. The value shown for structural damping was chosen to accelerate the decay of the transient solution, which is quite slow in the absence of structural damping, due to the small amount of aerodynamic damping present at 90,000 ft. As can be seen from Fig. 3, 5% structural damping has only a slight effect on the limit cycle behavior. However, as a practical consideration, the small amount of aerodynamic damping present at the high altitudes encountered for a hypersonic flight envelope may prove to be inadequate

for achieving stable limit cycles unless damping is augmented by artificial means.

A convergence study was carried out for a flat, unheated orthotropic panel and the results are shown in Fig. 8. The graph reveals interesting aspects of the convergence behavior of the solution at high values of post-critical dynamic pressure. The 8×1 mode solution can be considered to be converged. An examination of the modal coefficients reveals that the higher modes do not significantly contribute to the motion at the dynamic pressures that are plotted. The 6×1 mode solution is essentially converged, except for a small interval of dynamic pressure, $2400 < \lambda < 2850$. The 4×1 mode solution slightly underpredicts the value of λ_{cr}, and overpredicts the limit cycle amplitude for larger values of λ. At $\lambda = 1800$, the flutter oscillations for the 4×1 mode solution cease to be of constant amplitude and simple harmonic motion in time, and this is reflected in Fig. 8 by the erratic shape of the curve at values of λ above 1800. Similar behavior is observed in the region of λ for which the 6×1 mode solution is not converged.

It was found that the 8×1 mode solution also exhibits this behavior, albeit for very high values of λ. At values of post-critical dynamic pressure where the limit cycle curve is smooth, the panel oscillates with constant amplitude and with simple harmonic motion in time. The phase plane plot of the panel motion in this region is of an ellipse. Figures 9 and 10 show the change in the nature of the phase plane plot for the 8×1 mode solution for $\lambda = 5000$ and $\lambda = 6000$ respectively. Figure 9 reveals that the period has doubled and Fig. 10 reveals that the motion has become aperiodic. To determine if the 8×1 mode solution is converged for $\lambda = 5000$ and 6000, the equations were solved using 10×1 modes and 8×3 modes. Identical results were obtained, and an examination of the modal coefficients for the 8×1 mode solution revealed that the higher modes do not significantly contribute to the motion.

It appears that aperiodic motions occur for the flat, unheated orthotropic panel at sufficiently high λ. Similar behavior was recently observed by Hopkins and Dowell [27] for a cantilevered isotropic plate. This behavior has also been observed by the present authors for heated panels, where it occurs at values of λ that are significantly closer to λ_{cr} than for the case of the unheated panel. Further research is necessary to better understand this behavior.

To assess the influence of aerodynamic heating on the flutter behavior, the temperature distribution given by Eq. (13) was considered. Results are given for the orthotropic panel for the ratio of the temperature coefficient to the critical static buckling value of that coefficient. The static buckling values of the coefficients are given in the following table.

A_{T^*}	B_{T^*}	$C_{T^*}\&D_{T^*}$	E_{T^*}
9.55° F	1.97° F	3.94° F	7.88° F

The value of E_{T^*} is twice the value of C_{T^*} and D_{T^*}, and four times the value of B_{T^*}. These coefficients appear in the equations of motion through the coefficients of the homogeneous solution for $\bar{F}$, Eq.(20). This equation reveals that consideration of only one of these four coefficients is necessary, as the results for each will be identical.

The sinusoidal temperature distribution appears in the equations of motion through the coefficients of the homogeneous solution for $\bar{F}$, the particular solution for $\bar{F}$, and thermal moments if $s1 \neq 0$. Note that the actual coefficient of the sinusoidal temperature term is $A_T/2$ when $s1 = 0$. Furthermore, when $s1 = 1$, nonzero thermal moments are present in the panel and a unique buckling temperature does not exist. For this case results are presented with respect to the buckling temperature for $s1 = 0$.

Results for the uniform temperature distribution (and equivalently for the linear and bilinear distributions) are shown in Fig. 11 for values of B_T/B_{T^*} equal to 0, 0.5, and 1. Increasing the ratio has a strong destablizing effect on the panel. For the ratio of 1, the curves are very

steep and the aperiodic behavior described previously for the unheated panel occurs in the case of the heated panel; in this case for values of λ above about 350 for $B_T/B_{T^*} = 1$.

Results for the sinusoidal temperature distribution are shown in Fig. 12 for values of A_T/A_{T^*} equal to 0, 0.5, and 1, and for $s1 = 0$ and 1. For $s1 = 1.0$, the panel experiences a significant static deflection prior to the onset of flutter. The static deflection is due to the presence of thermal moment resultants in the equations of motion. For $A_T/A_{T^*} = 1.0$ and $s1 = 1.0$, a discontinuity exists in the curve at $\lambda_{cr} = 200$, indicating that the onset of flutter is quite sudden. The curve plotted is for values of λ for which the limit cycle oscillation remains simple harmonic. For $A_T/A_{T^*} = 1.0$ and $s1 = 0.0$, the curve is not smooth. A typical phase plane plot for this panel is shown in Fig. 13. Although the motion is periodic, it is not simple harmonic.

A panel located on the surface of a hypersonic vehicle will typically be exposed to flow aft of a shock caused by the vehicle shape rather than flow at its free stream conditions. Fig. 14 gives limit cycle curves for several values of flow deflection angle, which in this study is taken to be equal to the slope of the vehicle surface. As a useful reference value, a flow deflection angle of 3.6° is obtained if the the vertical cross section of the NASP Demonstrator model is approximated by a triangle with the dimensions given in [29]. It is apparent that the presence of a shock has a strong destablizing effect on the panel flutter, and larger flow deflection angles lead to lower critical dynamic pressures. Also, the slope of the limit cycle curve is considerably steeper when a shock is included in the formulation, indicating that the panel may experience damaging stress levels at post-critical dynamic pressures which are closer to the critical value than is the case when a shock is not included.

Initial curvature was incorporated into the model using Eq.(16) and the solution was obtained for various values of $\bar{Z}_{11}$. Fig. 16 shows the limit cycle curves for $\bar{Z}_{11} = 0, 0.5, 1.0, 1.5,$ and 2.0 for values of λ below the appearance of aperiodic motion. As can be seen from Eq. (10), nonzero initial curvature introduces a static forcing term into the aerodynamic load, resulting in significant nonzero static displacements at values of λ below λ_{cr}. In general, the presence of nonzero initial curvature seems to increase the stability of the simply supported panel, although the value of λ_{cr} is not a monotonically increasing function of initial panel height. For example, the value of λ_{cr} for $\bar{Z}_{11} = 1.0$ is 1560, which is significantly greater than the values of λ_{cr} for $\bar{Z}_{11} = 1.5$ and 2.0. Qualitatively similar results were obtained by Dowell [13] for the simply supported isotropic panel with constant curvature in the x- and y-directions.

6. Concluding Remarks

The flutter of a shallow curved orthotropic panel, undergoing moderate deflections in hypersonic flow at high altitudes was studied. The effects of dynamic pressure variations, temperature, and curvature, together with the location of the panel on the surface of a generic hypersonic vehicle.

Conventional thin panels appear to be quite sensitive to small temperature variations. Curvature also has an important influence on the dynamic behavior of panels. Exceeding the linear stability boundaries can lead to rapid increases in limit-cycle amplitudes, which may affect the structural integrity of a hypersonic vehicle.

The aerodynamic load obtained from piston theory differs substantially from that calculated from the solution of the complete Navier Stokes equations using CFD; for a prescribed time history of panel motion; which resembles the dynamics of a fluttering plate. Results based on third order piston theory can be quite inaccurate.

It is evident that the understanding of aeroelastic behavior in hypersonic flight requires considerable additional research.

Acknowledgement

This research was supported by NASA grant NCC-2-374 provided under the auspices of the UCLA/NASA Dryden Flight Systems Research Center. The useful comments of the grant monitor, Dr. K. Gupta, from Dryden are gratefully acknowledged.

References

[1] Ricketts, R., Noll, T., Whitlow, W., and Huttsell,L., "An Overview of Aeroelasticiey Studies for the National Aerospace Plane", AIAA Paper No. 93-1313, Proc. 34st AIAA/ASME/ASCE/AHS/ASC Structures, Structural Dynamics and Materials Conference, La Jolla, CA, April 19-22, 1993, pp. 152-162

[2] Spain, C. and Bullock, E., " A Flutter Investigation of All-Moveable NASP-Like Wings at Hypersonic Speeds", AIAA Paper No. 93-1315, Proc. 34st AIAA/ASME/ASCE/AHS/ASC Structures, Structural Dynamics and Materials Conference, La Jolla, CA, April 19-22, 1993

[3] Hegg, J., Zeiler, T., Pototzky, A., Spain, C., and Engelund, W., "Aerothermoelastic Analysis of a NASP Demonstrator Model", AIAA Paper No. 93-1366, Proc. 34st AIAA/ASME/ASCE/AHS/ASC Structures, Structural Dynamics and Materials Conference, La Jolla, CA, April 19-22, 1993, pp.617-627

[4] Zhou, R., Mei, C., and Xue, D., "A Finite Element Time Domain-Modal Formulation for Nonlinear Flutter of Composite Panels at Elevated Temperature,", AIAA Paper No. 94-1424, Proc. 35th AIAA/ASME/ASCE/AHS/ASC Structures, Structural Dynamics and Materials Conference, Hilton Head, S.C., April 18-20, 1994, pp.933-943

[5] Ashley, H. and Zartarian, G., "Piston Theory - A New Aerodynamic Tool for the Aeroelastician," *J. Aeronautical Science*, Vol. 23, No. 10, 1956, pp. 1109-1118

[6] Mei, C. and Grey, C., "A Finite Element Method for Large-Amplitude, Two-Dimensional Panel Flutter at Hypersonic Speeds,", AIAA Paper No. 89-1165, Proc. 30th AIAA/ASME/ASCE/AHS/ASC Structures, Structural Dynamics and Materials Conference, Mobile, AL, April 1989, pp. 37-51

[7] Xue, D.Y. and Mei, C., "Finite Element Two-Dimensional Panel Flutter at High Supersonic Speeds and Elevated Temperature,"AIAA Paper No. 09-0982, Proc. 31st AIAA/ASME/ASCE/AHS/ASC Structures, Structural Dynamics and Materials Conference, 1990, pp. 1464-1475

[8] Xue, D.Y. and Mei, C., "Finite Element Nonlinear Flutter and Fatigue Life of 2-D Panels with Temperature Effects,", AIAA Paper No. 91-1170, Proc. 32nd AIAA/ASME/ASCE/AHS/ASC Structures, Structural Dynamics and Materials Conference, Baltimore, MD, April 8-10,1991, pp. 1981-1991

[9] Abbas, J.F. and Ibrahim,R.A.,"Nonlinear Flutter of Orthotropic Composite Panel Under Aerodynamic Heating," *AIAA J.*, Vol. 31, No. 8, 1993, pp. 1478-1488

[10] Gray, E.G. and Mei, C., "Large-Amplitude Finite Element Flutter Analysis of Composite Panels in Hypersonic Flow," AIAA Paper No. 92-2130, Proc. 33rd AIAA/ASME/ASCE/AHS/ASC Structures, Structural Dynamics and Materials Conference, Dallas, TX, April 16-17, pp. 492-512

[11] Bein, T., Friedmann, P., Zhong, X., and Nydick, I., "Hypersonic Flutter of a Curved Shallow Panel with Aerodynamic Heating," AIAA Paper No. 93-1318, Proc. 34st AIAA/ASME/ASCE/AHS/ASC Structures,

Structural Dynamics and Materials Conference, La Jolla, CA, April 19-22, 1993

[12] Dowell, E.H., "Nonlinear Flutter of Curved Plates," *AIAA J.*, Vol. 7, No. 3, 1969, pp. 424-431

[13] Dowell, E.H., "Nonlinear Flutter of Curved Plates, II," *AIAA J.*, Vol. 8 No. 2, 1970, pp. 259-261

[14] Bismarck-Nasr, M.N., "Supersonic Panel Flutter Analysis of Shallow Shells," *AIAA J.*, Vol. 31, No. 7, pp. 1349-1351

[15] Pidaparti, R.M. and Yang, H., "Supersonic Flutter Analysis of Composite Plates and Shells," *AIAA J.*, Vol. 31, No. 6, pp. 1109-1117

[16] Marguerre, K., "Zur Theorie der Gekrummten Platte Grosser Formanderung," Proc. 5th International Congress on Applied Mechanics, 1938, pp. 93-101

[17] Anderson, J.D., *Modern Compressible Flow, with Historical Perspective*, McGraw-Hill, New York, 1990, p.106

[18] Anderson, J.D., *Hypersonic and High Temperature Gas Dynamics*, McGraw-Hill, New York, 1989, p.39

[19] Friedmann, P. and Hanin, M., "Supersonic Nonlinear Flutter of Orthotropic or Isotropic Panels with "Aribitrary" Flow Direction," *Israel Journal of Technology*, Vol. 6, No. 1-2, 1968, pp.46-57

[20] Librescu, L., "Aeroelastic stability of Orthotropic Heterogeneous Thin Panels in the Vicinity of the Flutter Critical Boundary," *Journal de Mecanique*, Vol.4, No. 1, pp. 51-76

[21] Dowell, E.H., "Nonlinear Oscillations of a Fluttering Plate," *AIAA J.*, Vol. 4, No. 7, 1966, pp. 1267-1275

[22] Dowell, E.H., *Aeroelasticity of Plates and Shells*, Noordhoff International Publishing, Lyden, The Netherlands, 1975.

[23] *Macsyma: System Reference Manual, Version 14*, Macsyma Inc., 1993

[24] Shampine, L.F. and Gordon, M.K., *Computer Solution of Ordinary Differential Equations*, W.H. Freeman and Co., San Francisco, 1975

[25] Harten, A., Engquist, B.,Osher, S., and Chakravarthy, S., "Uniformly High Order Accurate Essentially Non-Oscillatory schemes, III," *Journal of Computational Physics*, Vol. 71, No. 2, August 1987

[26] Zhong, X., "Application of Essentially Nonoscillatory Schemes to Unsteady Hypersonic Shock-Shock Interference Heating Problems," *AIAA J.*, Vol. 32, No. 8, 1994, pp. 1606-1616

[27] Hopkins, M.A. and Dowell, E.H., "Limited Amplitude Panel Flutter with a Temperature Differential", AIAA Paper No. AIAA-94-1486, Proc. 35th AIAA/ASME/ASCE/AHS/ASC Structures, Structural Dynamics and Materials Conference, Hilton Head, S.C., April 18-20, 1994, pp. 1343-1355

[28] Dowell, E.H., "Flutter of a Buckled Panel as an Example of Chaotic Motion of a Deterministic Autonomous System", *Journal of Sound and Vibration*, 1982, pp.333-344

[29] Soistmann, D. and Spain, C., "An Experimental and Analytical Study of a Lifting Body Wind Tunnel Model Exhibiting Body-Freedom Flutter," AIAA Paper No. 93-1316-CP, Proc. 34st AIAA/ASME/ASCE/AHS/ASC Structures, Structural Dynamics and Materials Conference, La Jolla, CA, April 19-22, 1993, pp. 171-181

	Isotropic	Orthotropic
a/b	1	1
a/h	240	300
E_y/E_x	1	0.6452
ν_{yx}	0.3	0.27
ν_{yx}/ν_{xy}	1	0.6452
M_∞	10	15
α_x	1.25×10^{-5}	n.a.
α_y/α_x	1	n.a.
altitude	n.a.	n.a
ρ_∞/ρ_0	4.167×10^{-3}	0.005
modes	6x1	8x1
order of piston theory	1	3
structural damping	0%	0%
ξ	0.75	0.75
η	0.5	0.5

Table 1: Data Used in the Validation Studies Shown in Figs. 5 and 6

	Isotropic	Orthotropic
a/b	1	1
a/h	500	500
E_y/E_x	1	20
ν_{yx}	0.3	0.3
ν_{yx}/ν_{xy}	1	20
M_∞	10	10
α_x	1.2×10^{-5}	2.1×10^{-5}
α_y/α_x	1	0.001
altitude	90,000 ft	90,000 ft
ρ_∞/ρ_0	1.071×10^{-5}	1.928×10^{-5}
modes	6x1	8x1
order of piston theory	3	3
structural damping	5%	5%
ξ	0.75	0.75
η	0.5	0.5

Table 2: Data Used in the Calculations

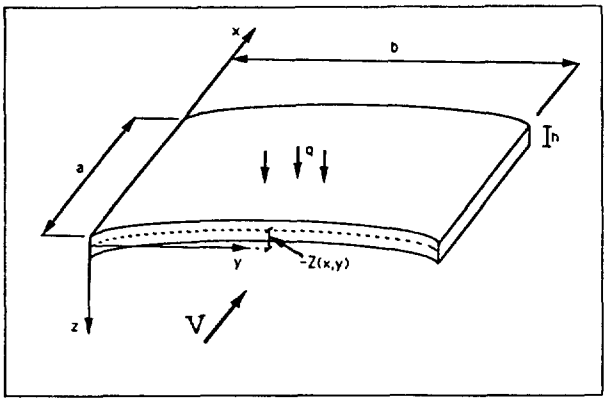

Figure 1: Definition of Panel Geometry

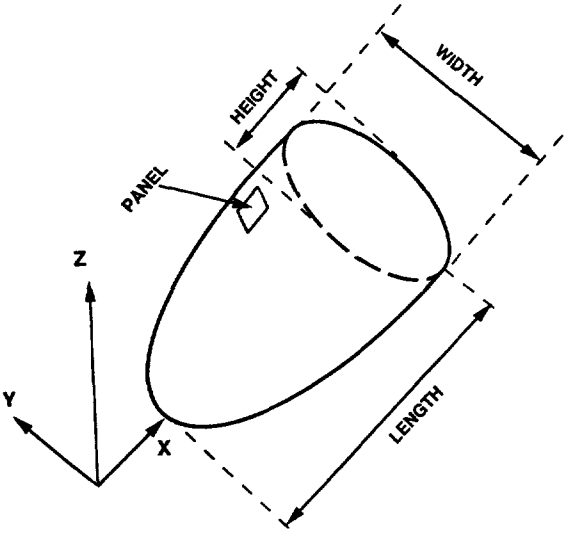

Figure 2: Generic hypersonic vehicle/panel combination

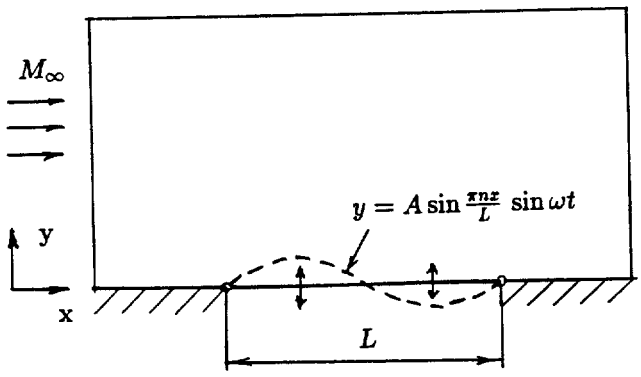

Figure 3: Schematic of the 2-D unsteady hypersonic flow field used to validate piston theory

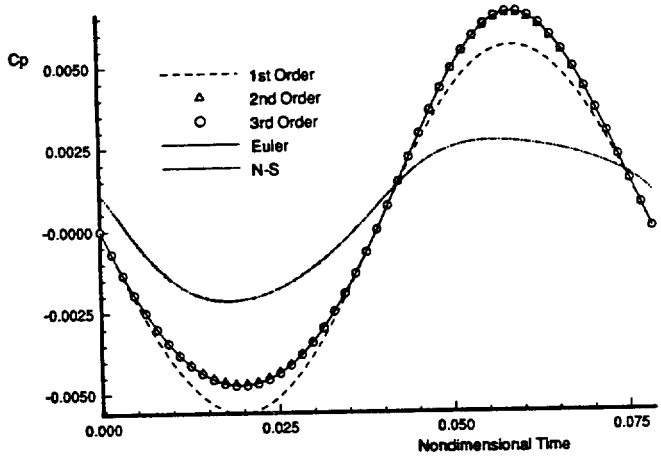

Figure 4: Pressure coefficient on the mid-panel surface as a function of nondimensional time ($\bar{t} = \omega t/80$).

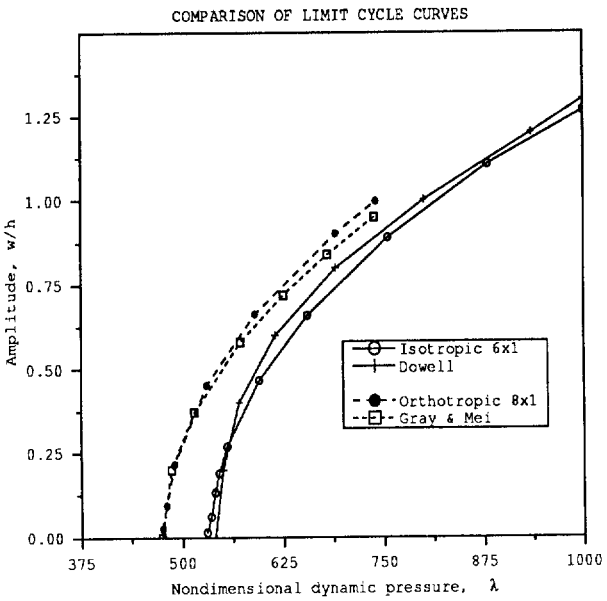

Figure 5: Unheated isotropic and orthotropic panels - comparison with previous research

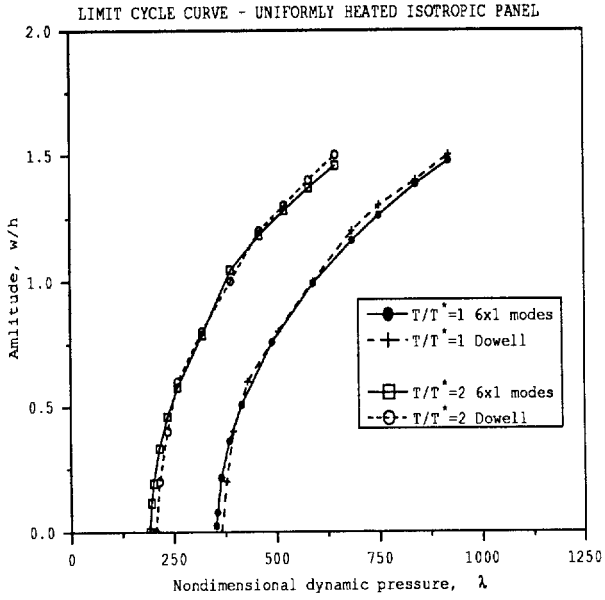

Figure 6: Uniformly heated isotropic panel - comparison with previous research

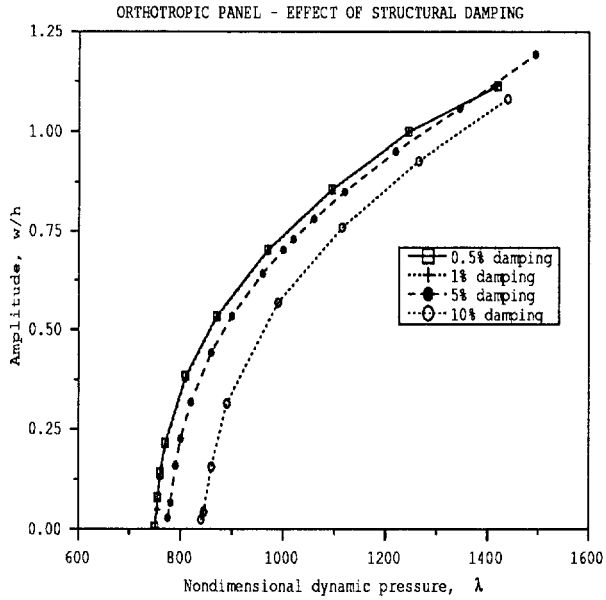

Figure 7: Effect of Structural Damping On Limit Cycles

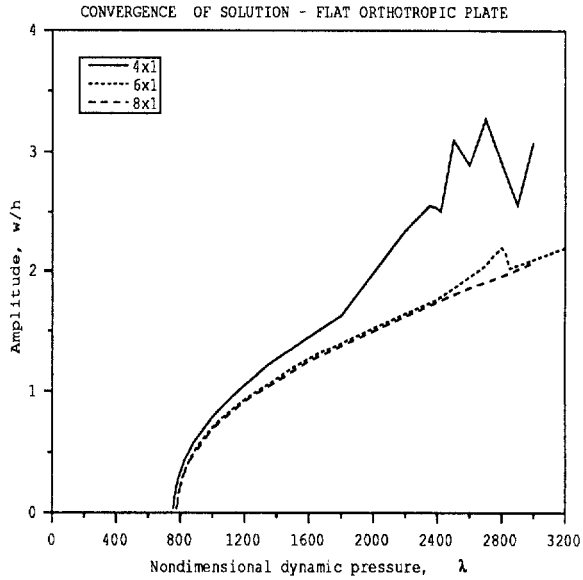

Figure 8: Convergence of the solution

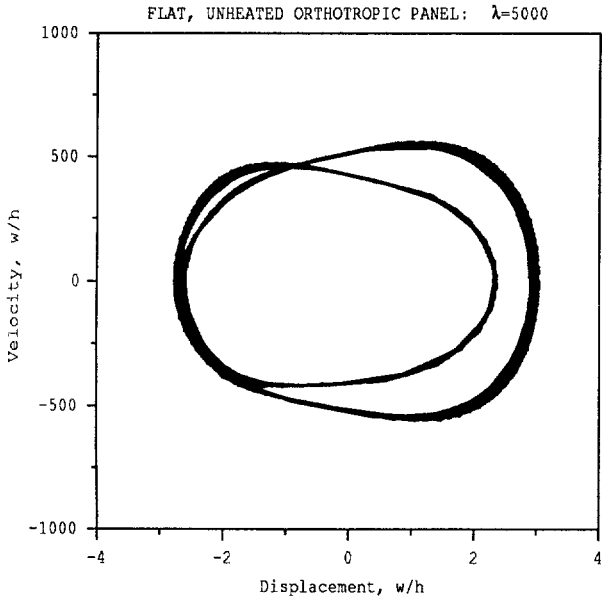

Figure 9: Phase plane plot of flat, unheated orthotropic panel for $\lambda = 5000$

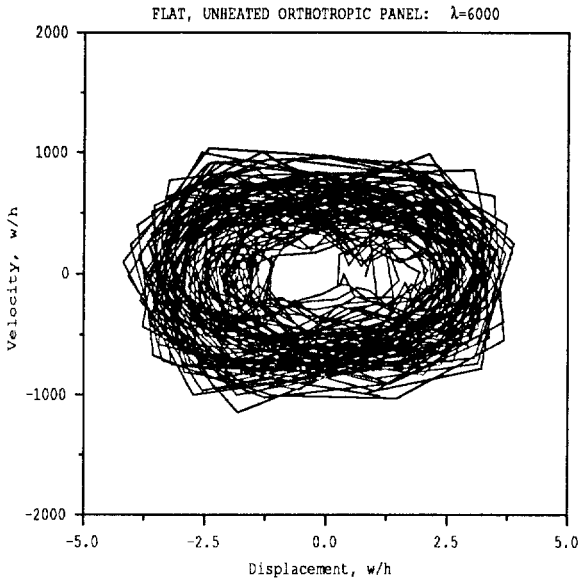

Figure 10: Phase plane plot of flat, unheated orthotropic panel for $\lambda = 6000$

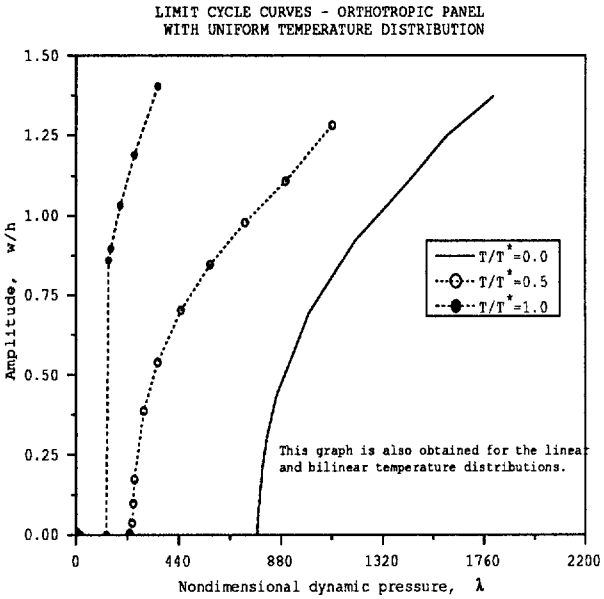

Figure 11: Effect of uniform temperature distribution - flat orthotropic panel

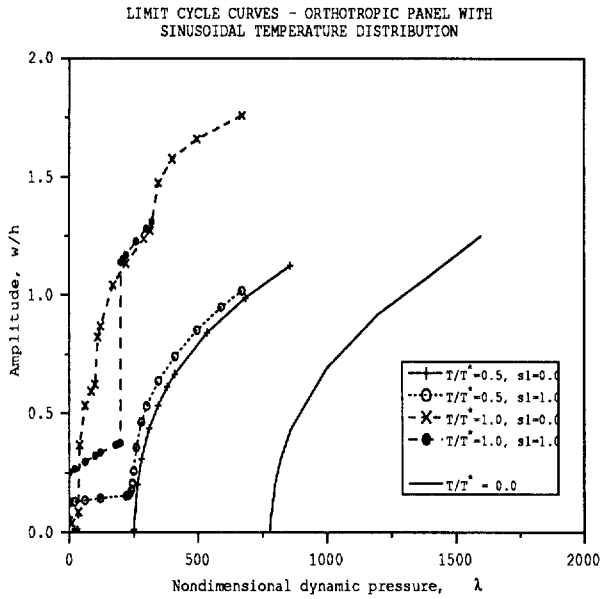

Figure 12: Effect of sinusoidal temperature distribution - flat orthotropic panel

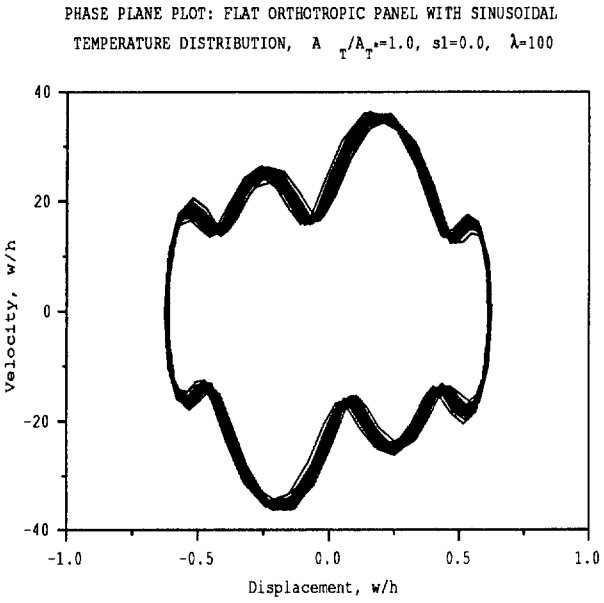

Figure 13: Phase plane plot of flat orthotropic panel with sinusoidal temperature distribution for $\lambda = 100,\ A_T/A_{T^*} = 1.0,\ s1 = 0$

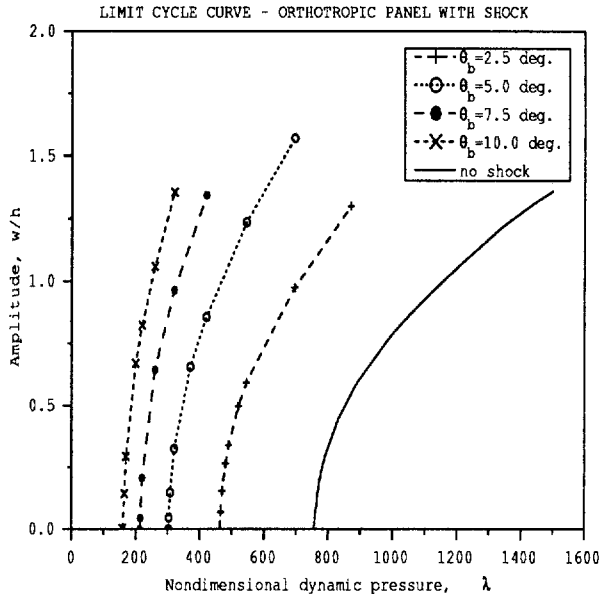

Figure 14: Effect of shock

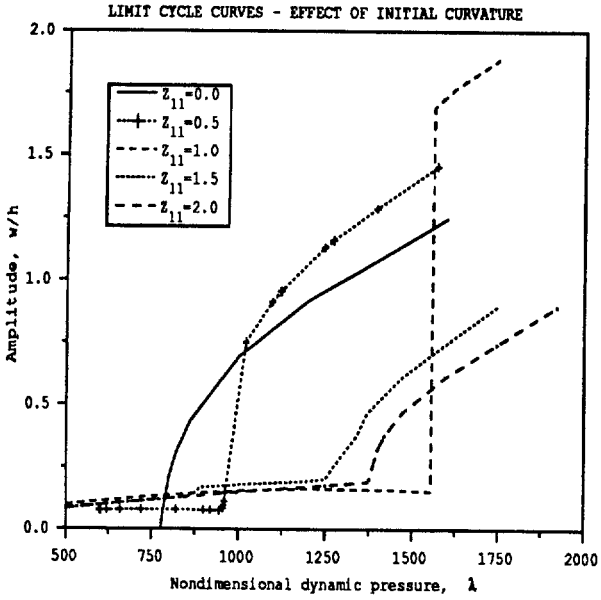

Figure 15: Effect of initial curvature as given by Eq.(16) - unheated orthotropic panel